Constraints on Single-Field Inflation from the BOSS Galaxy Survey

Giovanni Cabass,[1,*] Mikhail M. Ivanov,[1,†] Oliver H. E. Philcox ![ORCID],[2,1] Marko Simonović ![ORCID],[3] and Matias Zaldarriaga[1]

[1]*School of Natural Sciences, Institute for Advanced Study, 1 Einstein Drive, Princeton, New Jersey 08540, USA*
[2]*Department of Astrophysical Sciences, Princeton University, Princeton, New Jersey 08540, USA*
[3]*Theoretical Physics Department, CERN, 1 Esplanade des Particules, Geneva 23 CH-1211, Switzerland*

Nonlocal primordial non-Gaussianity (NLPNG) is a smoking gun of interactions in single-field inflationary models and can be written as a combination of the equilateral and orthogonal templates. We present the first constraints on these from the redshift-space galaxy power spectra and bispectra of the BOSS data. These are the first such measurements independent of the cosmic microwave background fluctuations. We perform a consistent analysis that includes all necessary nonlinear corrections generated by NLPNG and vary all relevant cosmological and nuisance parameters in a global fit to the data. Our conservative analysis yields joint limits on the amplitudes of the equilateral and orthogonal shapes, $f_{\rm NL}^{\rm equil} = 940 \pm 600$ and $f_{\rm NL}^{\rm ortho} = -170 \pm 170$ (both at 68% CL). These can be used to derive constraints on coefficients of the effective single-field inflationary Lagrangian; in particular, we find that the sound speed of inflaton fluctuations has the bound $c_s \geq 0.013$ at 95% CL. Fixing the quadratic galaxy bias and cosmological parameters, the constraints can be tightened to $f_{\rm NL}^{\rm equil} = 260 \pm 300$ and $f_{\rm NL}^{\rm ortho} = -23 \pm 120$ (68% CL).

Introduction.—Cosmology is the interface between particle physics and general relativity. Nothing exemplifies this more than inflation—a primordial accelerated expansion of the Universe that may have happened at energy scales as high as 10^{16} GeV. Inflation naturally generates quantum fluctuations that provide the seeds for the formation and clustering of matter and galaxies. Thus, observations of the large-scale structure of our Universe allow us to probe physics at these extremely high energies, inaccessible to present-day particle accelerators.

There are three main questions about inflation one may ask: What is its energy scale? How many degrees of freedom generated density fluctuations? How fast did these degrees of freedom propagate? While significant efforts have been devoted to answering the first question, by constraining the amplitude of primordial gravitational waves, the latter two require a probe of deviations of the initial density fluctuations from a Gaussian distribution, known as primordial non-Gaussianity (PNG).

The simplest observable encoding PNG is the bispectrum, B_ζ, of the primordial metric curvature perturbation ζ. Due to translational and rotational invariance, B_ζ is a function of the moduli of three momenta, $\mathbf{k}_1$, $\mathbf{k}_2$, $\mathbf{k}_3$, which form a closed triangle. A bispectrum peaking at squeezed triangles, $k_1 \ll k_2 \approx k_3$, is a generic signature of particle interactions in multifield inflation [1–10], but they typically produce strong PNG incompatible with data [12], i.e., where more than 1 degree of freedom is light during inflation. This type of PNG is called "local." In contrast, a bispectrum peaking at equilateral ($k_1 \approx k_2 \approx k_3$) or flattened ($k_1 \approx k_2 \approx k_3/2$) triangles is a peculiar feature of interactions in single-field inflation [13–20], which has only 1 degree of freedom (inflaton). This kind of "nonlocal" primordial non-Gaussianity (NLPNG) can be represented as a linear combination of two basis shapes, equilateral and orthogonal [20], with amplitudes $f_{\rm NL}^{\rm equil}$ and $f_{\rm NL}^{\rm ortho}$, respectively.

Symmetries of inflation also dictate a relationship between the inflaton speed of sound and the strength of nonlinear interactions that generate NLPNG [18]. In particular, there is a theorem stating that PNG can be large if and only if the sound speed is small [21,22]. This allows one to constrain the propagation speed of the inflaton from the observed level of NLPNG.

Up to now, the only source of information on NLPNG has been the cosmic microwave background (CMB) temperature and polarization data [12,23]. In particular, Planck 2018 data yield $f_{\rm NL}^{\rm equil} = -26 \pm 47$ and $f_{\rm NL}^{\rm ortho} = -38 \pm 24$ (both at 68% confidence level, hereafter CL) [12]. In theory, one can obtain better constraints with upcoming galaxy surveys, which will collect orders of magnitude more cosmological information as counted in the number

of accessible Fourier modes. However, the analysis of these data is also more intricate because PNG in the galaxy distribution is a weak effect on top of an intrinsic, late-time non-Gaussian signal generated by nonlinear clustering of matter. Thus, late-time nonlinearities act as background noise, which must be accurately modeled if we are to measure PNG from large-scale structure data.

There have been significant efforts to probe *local* PNG from galaxy surveys, exploiting the scale-dependent bias that enhances the observed power spectrum on very large scales [24–26]. This enhancement originates from a particular form of the squeezed limit of the local shape. NLPNG is different as the relevant shapes are suppressed in the squeezed limit and hence do not produce significant scale-dependent bias. Thus, this type of PNG requires a dedicated study. Indeed, the leading effect of NLPNG on galaxy clustering is a specific shape dependence in the galaxy bispectrum, which also modulates power spectra through loop corrections. These effects can be constrained by a systematic analysis based on the consistently modeled power spectrum and bispectrum data. In this Letter, we present the first such analysis of the publicly available state-of-the-art redshift clustering data from the Baryon Oscillation Spectroscopic Survey (BOSS).

A rigorous analysis of the galaxy bispectrum has been a challenge for a long time. Even ignoring PNG, the complete theoretical model including all necessary effects relevant for the actual data has been developed only recently [27,28] (see also Refs. [29–41]). On the data side, a major improvement has come from the estimators that remove effects of the survey window function [42,43]. These efforts now allow us to obtain the first CMB-independent limits on NLPNG from galaxy redshift surveys.

PNG in single-field inflation.—A general single-field Lagrangian for the inflaton perturbation π with leading interactions up to cubic order is given by [18,20]

$$S_{\mathrm{EFT}} = \int d^4x \sqrt{-g} \left[-\frac{M_{\mathrm{P}}^2 \dot{H}}{c_s^2} \left(\dot{\pi}^2 - c_s^2 \frac{(\nabla \pi)^2}{a^2} \right) + \frac{M_{\mathrm{P}}^2 \dot{H}}{c_s^2} (1 - c_s^2) \left(\frac{\dot{\pi}(\nabla \pi)^2}{a^2} - \left(1 + \frac{2}{3} \frac{\tilde{c}_3}{c_s^2} \right) \dot{\pi}^3 \right) \right]. \quad (1)$$

Here, π is related to the metric curvature perturbation via $\zeta = -H\pi$, with H being the Hubble parameter during inflation. The two inflaton interactions are parametrized by the sound speed c_s and a dimensionless Wilson coefficient $\tilde{c}_3$. It is customary to represent PNG produced by these interactions as a linear combination of the orthogonal and equilateral templates. To that end, we define

$$B_\zeta(k_1, k_2, k_3) = \frac{18}{5} f_{\mathrm{NL}} \Delta_\zeta^4 \frac{S(k_1, k_2, k_3)}{k_1^2 k_2^2 k_3^2}. \quad (2)$$

Here, Δ_ζ^2 is the amplitude of the primordial power spectrum: $k^3 P_\zeta(k) = \Delta_\zeta^2 (k/k_*)^{n_s-1}$, where n_s is the spectral index. Analysis of Planck data finds $\Delta_\zeta^2 \approx 4.1 \times 10^{-8}$, $n_s \approx 0.96$ [44] for the pivot scale $k_* = 0.05$ Mpc^{-1}. The equilateral and orthogonal templates are defined as [20,45,46]

$$S_{\mathrm{equil}}(k_1, k_2, k_3) = \left(\frac{k_1}{k_2} + 5 \,\mathrm{perms} \right) - \left(\frac{k_1^2}{k_2 k_3} + 2 \,\mathrm{perms} \right) - 2,$$

$$S_{\mathrm{ortho}}(k_1, k_2, k_3) = (1+p) \frac{\Delta}{e_3} - p \frac{\Gamma^3}{e_3^2}, \quad (3)$$

where $p = 8.52587$, $\Delta = (k_T - 2k_1)(k_T - 2k_2)(k_T - 2k_3)$,

$$k_T = k_1 + k_2 + k_3, \qquad e_2 = k_1 k_2 + k_2 k_3 + k_1 k_3,$$

$$e_3 = k_1 k_2 k_3, \qquad \Gamma = \frac{2}{3} e_2 - \frac{1}{3} (k_1^2 + k_2^2 + k_3^2). \quad (4)$$

The amplitudes $f_{\mathrm{NL}}^{\mathrm{equil}}$ and $f_{\mathrm{NL}}^{\mathrm{ortho}}$ are related to the coefficients of the EFT Lagrangian via [20,45]

$$\begin{pmatrix} f_{\mathrm{NL}}^{\mathrm{equil}} \\ f_{\mathrm{NL}}^{\mathrm{ortho}} \end{pmatrix} = \begin{pmatrix} 1.04021 & 1.21041 \\ -0.0395140 & -0.175685 \end{pmatrix} \begin{pmatrix} f_{\mathrm{NL}}^{\dot{\pi}(\nabla \pi)^2} \\ f_{\mathrm{NL}}^{\dot{\pi}^3} \end{pmatrix},$$

$$f_{\mathrm{NL}}^{\dot{\pi}(\nabla \pi)^2} = \frac{85}{324} (1 - c_s^{-2}),$$

$$f_{\mathrm{NL}}^{\dot{\pi}^3} = \frac{10}{243} (1 - c_s^{-2}) \left(\tilde{c}_3 + \frac{3}{2} c_s^2 \right). \quad (5)$$

Large-scale structure in the presence of NLPNG.—Before considering NLPNG, we first discuss structure formation in a universe with Gaussian initial conditions. We describe it in the framework of the effective field theory of large-scale structure (EFTofLSS), where one builds a perturbative expansion in terms of the linear matter overdensity field $\delta^{(1)}$ (see Refs. [34,35,47–50] and references therein). For Gaussian initial conditions, statistical properties of $\delta^{(1)}$ are fully determined by its power spectrum [51] P_{11},

$$\langle \delta^{(1)}(\mathbf{k}) \delta^{(1)}(\mathbf{k}') \rangle = (2\pi)^3 \delta_D^{(3)}(\mathbf{k}' + \mathbf{k}) P_{11}(k). \quad (6)$$

We restrict our galaxy power spectrum analysis to the one-loop order in the EFTofLSS. In the absence of NLPNG, the nonlinear power spectrum takes the following schematic form:

$$P_G \equiv P_{11} + P_{1-\mathrm{loop}} + P_{\mathrm{ctr}} + P_{\mathrm{stoch}}, \quad (7)$$

where $P_{1-\mathrm{loop}}$ is the nonlinear one-loop correction for Gaussian initial conditions, P_{ctr} is the counterterm that stems from the higher-derivative operators in the fluid equation and the bias expansion, while P_{stoch} captures galaxy stochasticity. Nonlinear clustering also generates a

nontrivial "Gaussian" bispectrum B_G, which we consider here in the tree-level approximation.

PNG affects large-scale structure via three channels: initial conditions, loop corrections, and scale-dependent galaxy bias. First, PNG induces a bispectrum signal in addition to the one coming from nonlinear mode coupling [52,53],

$$\langle \delta^{(1)} \delta^{(1)} \delta^{(1)} \rangle = f_\mathrm{NL} B_{111}(k_1, k_2, k_3)(2\pi)^3 \delta_D^{(3)}(\mathbf{k}_{123}),$$

$$f_\mathrm{NL} B_{111}(k_1, k_2, k_3) = \mathcal{T}(k_1)\mathcal{T}(k_2)\mathcal{T}(k_3) B_\zeta(k_1, k_2, k_3), \quad (8)$$

where $\mathbf{k}_{123} = \mathbf{k}_1 + \mathbf{k}_2 + \mathbf{k}_3$, and we introduced the transfer functions $\mathcal{T}(k) \equiv \delta^{(1)}(\mathbf{k})/\zeta(\mathbf{k}) = (P_{11}(k)/P_\zeta(k))^{1/2}$. The initial bispectrum (8) also leaks into the nonlinear galaxy power spectra through mode coupling, and it induces the following non-Gaussian one-loop correction (which adds to P_G above):

$$f_\mathrm{NL} P_{12}(\mathbf{k}) = 2 f_\mathrm{NL} Z_1(\mathbf{k}) \int \frac{\mathrm{d}^3 q}{(2\pi)^3} Z_2(\mathbf{q}, \mathbf{k} - \mathbf{q})$$
$$\times B_{111}(k, q, |\mathbf{k} - \mathbf{q}|). \quad (9)$$

Here, $Z_{1,2}$ are linear and quadratic galaxy redshift-space kernels [54] (see also the Supplemental Material [55]), and $Z_1(\mathbf{k}) = b_1 + f(\hat{\mathbf{k}} \cdot \hat{\mathbf{z}})^2$, where f is the logarithmic growth factor, $\hat{\mathbf{z}}$ is the line-of-sight direction unit vector, and $\hat{\mathbf{k}} \equiv \mathbf{k}/k$. The P_{12} terms are present for both galaxies and matter [56–58], and we refer to them as "NG matter loops" in what follows.

Third, NLPNG modulates galaxy formation, which is captured on large scales by the scale-dependent galaxy bias [49,59–61],

$$\delta_g = b_1 \delta + f_\mathrm{NL} b_\zeta (k/k_\mathrm{NL})^2 \zeta + \text{nonlinear}, \quad (10)$$

where δ and δ_g are overdensity fields of matter and galaxies, respectively; b_1 is the usual linear bias; b_ζ is an order-one PNG linear bias coefficient; and $k_\mathrm{NL} \approx 0.5 \, h \, \mathrm{Mpc}^{-1}$ is the nonlinear scale [62] at the relevant redshift $z \simeq 0.5$.

The relative size of various perturbative corrections can be estimated using the scaling universe approach [57,63]. It is based on the observation that the linear power spectrum can be well approximated by a power-law $P_{11} \propto (k/k_\mathrm{NL})^n k_\mathrm{NL}^{-3}$ with $n \approx -1.7$ for quasilinear wave numbers $k \simeq 0.15 \, h \, \mathrm{Mpc}^{-1}$. Assuming that there is a single nonlinear scale in the problem, the scaling universe estimates suggest that the leading non-Gaussian corrections are the PNG matter loops and the linear scale-dependent bias. The total dimensionless galaxy power spectrum $\Delta^2(k) \equiv k^3 P(k)/(2\pi^2)$ can be estimated as

$$\Delta^2(k) = \underbrace{\left(\frac{k}{k_\mathrm{NL}}\right)^{1.3}}_{\text{tree}} + \underbrace{\left(\frac{k}{k_\mathrm{NL}}\right)^{2.6}}_{\text{1–loop}} + \underbrace{\left(\frac{k}{k_\mathrm{NL}}\right)^{3.3}}_{\text{ctr}} + \underbrace{\left(\frac{k}{k_\mathrm{NL}}\right)^{3}}_{\text{stoch}}$$
$$+ \underbrace{f_\mathrm{NL} \Delta_\zeta \left(\frac{k}{k_\mathrm{NL}}\right)^{1.95}}_{\text{NG matter loops}} + \underbrace{f_\mathrm{NL} b_\zeta \Delta_\zeta \left(\frac{k}{k_\mathrm{NL}}\right)^{2.65}}_{\text{linear PNG bias}}. \quad (11)$$

All higher order corrections—such as PNG terms $\mathcal{O}(f_\mathrm{NL}^2)$, NG two-loop corrections, contributions generated by non-linear bias operators like $\delta \nabla^2 \zeta$, and Gaussian two-loop corrections—are subleading for $f_\mathrm{NL} \Delta_\zeta \lesssim 0.1$ and $k \lesssim 0.17 \, h \mathrm{Mpc}^{-1}$ typical for our analysis and hence can be neglected [64]. This will be validated on the mock simulation data below. As for the bispectrum, we use the tree-level approximation, so only the leading PNG bispectrum (8) is of importance [57]. See also the Supplemental Material [55].

All in all, our final model for the galaxy power spectra and bispectra in redshift space is given by

$$P(\mathbf{k}) = P_\mathrm{G}(\mathbf{k}) + f_\mathrm{NL}\left(P_{12}(\mathbf{k}) + \frac{2b_\zeta Z_1(\mathbf{k})k^2}{k_\mathrm{NL}^2} \frac{P_{11}(k)}{\mathcal{T}(k)}\right),$$

$$B(\mathbf{k}_1, \mathbf{k}_2, \mathbf{k}_3) = B_\mathrm{G}(\mathbf{k}_1, \mathbf{k}_2, \mathbf{k}_3) + f_\mathrm{NL} Z_1(\mathbf{k}_1) Z_1(\mathbf{k}_2) Z_1(\mathbf{k}_3)$$
$$\times B_{111}(k_1, k_2, k_3), \quad (12)$$

where P_G and B_G are the standard Gaussian power spectrum and bispectrum models [27,65]. In practice, we compute the Legendre redshift-space multipoles P_ℓ ($\ell = 0, 2, 4$) of the galaxy power spectrum and use the angle-averaged (monopole) bispectrum. We also implement ir resummation in redshift space [66–71] (to account for long-wavelength displacement effects) and the Alcock-Paczynski effect [72] (to account for coordinate conversions [34]).

Our model has 14 nuisance parameters: 13 standard bias parameters and counterterms of Gaussian redshift-space power spectra and bispectra (present in previous analyses), plus the scale-dependent PNG bias b_ζ (10).

Data and analysis.—We use the twelfth data release (DR12) [73] of BOSS. The data are split into two redshift bins with effective means $z = 0.38$ and 0.61, in each of the Northern and Southern Galactic Caps, resulting in four independent data chunks. The survey contains $\sim 1.2 \times 10^6$ galaxy positions with a total volume of $6(h^{-1} \, \mathrm{Gpc})^3$. From each chunk, we use the power spectrum multipoles ($\ell = 0, 2, 4$) for $k \in [0.01, 0.17] \, h\mathrm{Mpc}^{-1}$, the real-space power spectrum Q_0 for $k \in [0.17, 0.4] \, h\mathrm{Mpc}^{-1}$ [74], the redshift-space bispectrum monopoles for triangle configurations within the range of $k_i \in [0.01, 0.08) \, h\mathrm{Mpc}^{-1}$ (62 triangles), and the BAO parameters extracted from the post-reconstructed power spectrum data [75], as in Ref. [28]. The power spectra and bispectra are measured with the window-free estimators [42,43]. The covariances for each

data chunk are computed from a suite of 2048 MultiDark-Patchy mocks [76].

We perform the full-shape analysis of the red-shift clustering data following the methodology of Refs. [28,34,35,75]. We implement the complete theory model for the power spectra and bispectra of galaxies in redshift space in an extension of the CLASS-PT code [54] that includes all non-Gaussian corrections described above (computed using the FFTlog approach [77]). We consistently recompute the shape of these corrections as we scan over different cosmologies in a Markov chain Monte Carlo (MCMC) analysis. Up to additional NG contributions, our analysis is identical to Ref. [28].

In our baseline analysis we fix the baryon density to the BBN measurement [78], the primordial power spectrum tilt to the Planck best-fit value [44], and the neutrino mass to the minimal value allowed by oscillation experiments, $\sum m_\nu = 0.06$ eV. We vary the physical dark matter density ω_{cdm}, the reduced Hubble parameter h, the amplitude of the primordial scalar fluctuations $\ln(10^{10} A_s)$, and $(f_{NL}^{equil}, f_{NL}^{ortho})$ within flat, infinitely wide priors. We use the same priors for nuisance parameters as in Ref. [28]. We also marginalize over the linear PNG bias, $b_\zeta = 1.686 \times (18/5)(b_1 - 1)\tilde{b}_\zeta$ within a Gaussian prior $\tilde{b}_\zeta \sim \mathcal{N}(1, 5)$ motivated by the peak-background split model [79].

In addition, we perform a more aggressive analysis, whereupon cosmological parameters are set to the Planck 2018 priors. Moreover, instead of marginalization, we fix the quadratic galaxy biases to predictions of the standard dark matter halo relations [49] (see also the Supplemental Material [55]). These agree with simulations at the level required by the BOSS data [27,37].

It is worth noting that our analysis is different from the CMB one [20], where f_{NL} is estimated directly from the temperature and polarization maps. In contrast, we do a global fit to the summary statistics and vary f_{NL}^{equil} and f_{NL}^{ortho} along with all other cosmological and nuisance parameters in our MCMC chains, which is necessary due to the appearance of parameter-dependent late-time non-Gaussianity.

Results.—First, we apply our pipeline to Nseries mock catalogs. These are based on high-resolution N-body simulations and were used by the BOSS Collaboration for validation tests [73]. The cumulative volume of this simulation is $235(h^{-1} \text{ Gpc})^3$, which is approximately 40 times larger than actual BOSS survey volume.

The mocks were generated from purely Gaussian initial conditions, which we must recover with our pipeline as a consistency check. Note that our chains explore values of f_{NL} that are not zero; hence, the most rigorous validation of the pipeline requires tests on simulations with nonzero f_{NL}. This is an important point that will be addressed in future work [80]. Since our pipeline contains all necessary theoretical ingredients, we expect it to correctly recover
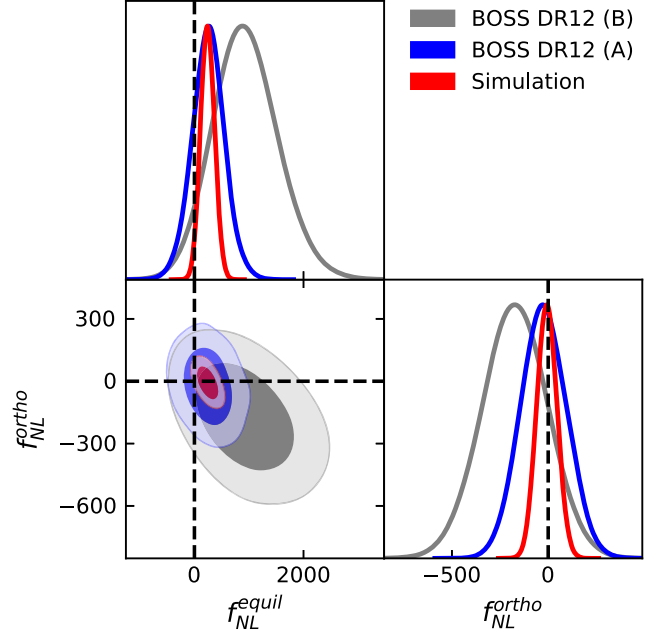

FIG. 1. Marginalized constraints on parameters $(f_{NL}^{equil}, f_{NL}^{ortho})$ from the BOSS data obtained in the conservative baseline analysis [BOSS DR12 (B), gray] and in the aggressive analysis [BOSS DR12 (A), blue]. We also show results from the full Nseries simulation suite (red), whose volume is 40 times larger than BOSS. Dashed lines indicate $f_{NL}^{equil} = 0$, $f_{NL}^{ortho} = 0$.

any input f_{NL}. Indeed, we find $f_{NL}^{equil} = 240_{-130}^{+130}$ and $f_{NL}^{ortho} = -6_{-54}^{+52}$, which is consistent with $f_{NL}^{equil} = 0$ within 95% CL and $f_{NL}^{ortho} = 0$ within 68% CL. The shift in f_{NL}^{equil}, even if statistically insignificant, yields an estimate of the theoretical uncertainty, $\Delta f_{NL}^{equil} \lesssim 100$, which is less than 0.2σ of the BOSS 1D marginalized statistical error. This is consistent with estimates of higher order perturbative corrections that are omitted in our analysis. We have also found that the constraints are driven by the bispectrum: the power spectrum data alone give $f_{NL}^{equil} = -640 \pm 1200$ and $f_{NL}^{ortho} = 2400 \pm 1600$ (at 68% CL).

Having validated our method on the simulations, we move to the actual BOSS data. Our baseline MCMC analysis yields the following 1D marginalized estimates of equilateral and orthogonal f_{NL} values from the joint fit:

$$f_{NL}^{equil} = 940_{-650}^{+570}, \quad f_{NL}^{ortho} = -170_{-170}^{+180} \quad (68\% \text{ CL}). \quad (13)$$

We do not find any evidence for NLPNG: the 95% CL limits read

$$-280 < f_{NL}^{equil} < 2190, \qquad -520 < f_{NL}^{ortho} < 176. \quad (14)$$

The resulting posterior contours are shown in Fig. 1. The correlation coefficient between the equilateral and orthogonal shapes is -0.40. The best-measured principal component is

$$f_{\mathrm{NL}}^{\mathrm{ortho}} - 0.11 f_{\mathrm{NL}}^{\mathrm{equil}} = -65 \pm 157.$$

Note that the correlation is dictated by degeneracy directions in the shape of the BOSS galaxy bispectrum. This can be contrasted with the Planck 2018 data that do not show any appreciable degeneracy between the two shapes; i.e., their correlation matches the intrinsic template cosine [12]. This implies that combinations with the CMB data will be important for degeneracy breaking in future analyses.

Our aggressive analysis yields noticeably stronger constraints, $f_{\mathrm{NL}}^{\mathrm{equil}} = 257_{-300}^{+300}$ and $f_{\mathrm{NL}}^{\mathrm{ortho}} = -23_{-120}^{+120}$. Most of the improvement here is driven by fixing quadratic bias parameters. In light of the well-known σ_8 tension, we have also varied σ_8 in our aggressive fit, which somewhat loosens the bounds, $f_{\mathrm{NL}}^{\mathrm{equil}} = 510_{-440}^{+320}$ and $f_{\mathrm{NL}}^{\mathrm{ortho}} = -123_{-140}^{+150}$ ($\sigma_8 = 0.728_{-0.037}^{+0.033}$), at 68% CL. Concluding, we emphasize that our aggressive analysis is performed mainly for the purposes of illustration. It demonstrates that PNG constraints can be significantly improved with a better knowledge of bias parameters, which motivates further work on their calibration with simulations, e.g., along the lines of Refs. [81,82].

We have also repeated our baseline analysis with free n_s and found consistent, albeit somewhat weaker limits $f_{\mathrm{NL}}^{\mathrm{equil}} = 1200_{-850}^{+630}$ and $f_{\mathrm{NL}}^{\mathrm{ortho}} = -240_{-180}^{+210}$ (with $n_s = 0.83 \pm 0.08$).

Constraints on early Universe physics.—Our main analysis was performed using flat priors on $f_{\mathrm{NL}}^{\mathrm{equil}}$ and $f_{\mathrm{NL}}^{\mathrm{ortho}}$, which map onto nonflat priors of the physical coefficients in the EFT Lagrangian (1). To avoid any potential prior bias, we repeat our MCMC analysis by directly varying the relevant parameters $\log_{10} c_s$ and $\tilde{c}_3(c_s^{-2} - 1)$ (following Ref. [20]), assuming flat priors $\log_{10} c_s \in (-\infty, 0]$ and $\tilde{c}_3(c_s^{-2} - 1) \in (-\infty, +\infty)$. The corresponding posterior contours are shown in Fig. 2. They yield the bound on the sound speed,

$$c_s \geq 0.013 \quad (\tilde{c}_3 \text{ marginalized}, 95\% \text{ CL}). \quad (15)$$

For DBI inflation [14], where $\tilde{c}_3 = 3(1 - c_s^2)/2$, we find $c_s \geq 0.04$ (95% CL). In general, the parameter $\tilde{c}_3$ cannot be constrained because of degeneracy with c_s; i.e., $\tilde{c}_3$ is unbounded in the limit $c_s \to 1$, where we can only constrain the combination of the two parameters,

$$-3.5 \times 10^4 < \tilde{c}_3(c_s^{-2} - 1) < 1 \times 10^4 \quad (95\% \text{ CL}). \quad (16)$$

Constraints on c_s do not noticeably improve with the aggressive analysis settings. This is because the ($f_{\mathrm{NL}}^{\mathrm{equil}}$, $f_{\mathrm{NL}}^{\mathrm{ortho}}$) parameter space excluded by these settings mostly corresponds to the unphysical values $c_s^2 > 1$, $c_s^2 < 0$, and hence does not contribute to our final constraints on this parameter [83].

Conclusions.—In this Letter we have presented the first non-CMB constraints on nonlocal primordial non-Gaussianity, using the BOSS redshift-space clustering data. Our nominal constraints on the orthogonal shape and the inflaton sound speed are competitive with those from the Wilkinson Microwave Anisotropy Probe CMB data [23]. These constraints will certainly improve with the data from upcoming surveys such as Euclid [84] or DESI [85]. Based on their volume with respect to BOSS, one may expect a reduction of error bars by a factor of 3. However, the limits from current and future surveys can be improved even further if more bispectrum data are used, e.g., from new triangles with larger wave numbers and from the angular dependence captured by higher order harmonics (multipoles) of the redshift-space bispectrum [86]. To achieve this, we will compute the one-loop bispectrum and the two-loop power spectrum corrections. In addition, as discussed above, the constraints can be improved with tighter priors on galaxy bias parameters, which can be extracted from realistic hydrodynamical simulations. We leave this information for future work. In addition, it would be interesting to analyze more complex PNG scenarios and also include information from the recently measured BOSS galaxy trispectrum [87].

Finally, it is worth noting that the PNG constraints from large-scale structure will further improve with futuristic surveys, such as MegaMapper [88] and 21 cm/intensity mapping observations, which will map our Universe at high redshifts where the late-time non-Gaussian clustering background is weak.
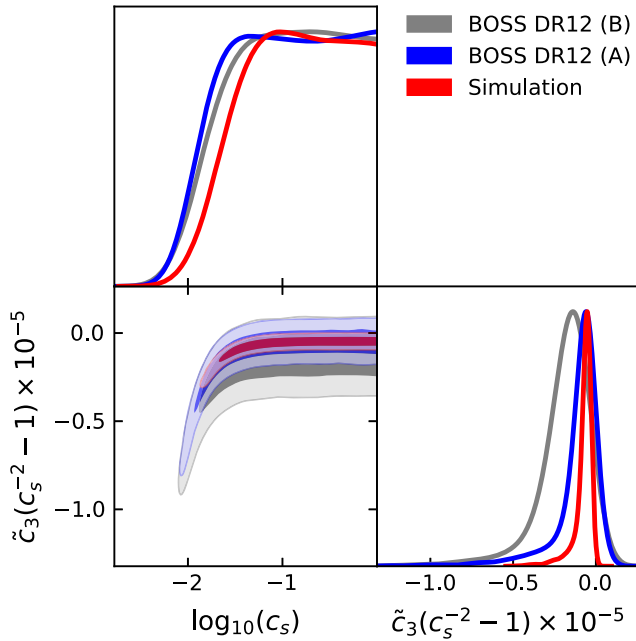

FIG. 2. Marginalized constraints on single-field inflation parameters (c_s, $\tilde{c}_3$) from the BOSS data in the baseline analysis [BOSS DR12 (B), gray], aggressive analysis [BOSS DR12 (A), blue], and from the full Nseries simulation suite (red).

Our work thus serves as a proof of principle and paves the way toward systematic analyses of PNG with upcoming large-scale structure surveys.

Code available at [89], with custom MontePython likelihoods available at [89].

*gcabass@ias.edu
†ivanov@ias.edu

[1] A. D. Linde and V. F. Mukhanov, Phys. Rev. D **56**, R535 (1997).
[2] K. Enqvist and M. S. Sloth, Nucl. Phys. **B626**, 395 (2002).
[3] D. H. Lyth and D. Wands, Phys. Lett. B **524**, 5 (2002).
[4] D. H. Lyth, C. Ungarelli, and D. Wands, Phys. Rev. D **67**, 023503 (2003).
[5] G. Dvali, A. Gruzinov, and M. Zaldarriaga, Phys. Rev. D **69**, 023505 (2004).
[6] G. Dvali, A. Gruzinov, and M. Zaldarriaga, Phys. Rev. D **69**, 083505 (2004).
[7] M. Zaldarriaga, Phys. Rev. D **69**, 043508 (2004).
[8] C. T. Byrnes and K.-Y. Choi, Adv. Astron. **2010**, 724525 (2010).
[9] L. Senatore and M. Zaldarriaga, J. High Energy Phys. 04 (2012) 024.
[10] These shapes also appear in ekpyrotic alternatives to inflation (see Ref. [11] for a review.
[11] J.-L. Lehners, Adv. Astron. **2010**, 903907 (2010).
[12] Y. Akrami et al. (Planck Collaboration), Astron. Astrophys. **641**, A9 (2020).
[13] N. Arkani-Hamed, P. Creminelli, S. Mukohyama, and M. Zaldarriaga, J. Cosmol. Astropart. Phys. 04 (2004) 001.
[14] M. Alishahiha, E. Silverstein, and D. Tong, Phys. Rev. D **70**, 123505 (2004).
[15] L. Senatore, Phys. Rev. D **71**, 043512 (2005).
[16] X. Chen, M.-x. Huang, S. Kachru, and G. Shiu, J. Cosmol. Astropart. Phys. 01 (2007) 002.
[17] P. Creminelli, M. A. Luty, A. Nicolis, and L. Senatore, J. High Energy Phys. 12 (2006) 080.
[18] C. Cheung, P. Creminelli, A. L. Fitzpatrick, J. Kaplan, and L. Senatore, J. High Energy Phys. 03 (2008) 014.
[19] C. Cheung, A. L. Fitzpatrick, J. Kaplan, and L. Senatore, J. Cosmol. Astropart. Phys. 02 (2008) 021.
[20] L. Senatore, K. M. Smith, and M. Zaldarriaga, J. Cosmol. Astropart. Phys. 01 (2010) 028.
[21] D. Baumann, D. Green, H. Lee, and R. A. Porto, Phys. Rev. D **93**, 023523 (2016).
[22] D. Green and E. Pajer, J. Cosmol. Astropart. Phys. 09 (2020) 032.
[23] C. L. Bennett et al., Astrophys. J. **208**, 20 (2013).
[24] B. Leistedt, H. V. Peiris, and N. Roth, Phys. Rev. Lett. **113**, 221301 (2014).
[25] E. Castorina et al., J. Cosmol. Astropart. Phys. 09 (2019) 010.
[26] E.-M. Mueller et al., arXiv:2106.13725.
[27] M. M. Ivanov, O. H. E. Philcox, T. Nishimichi, M. Simonović, M. Takada, and M. Zaldarriaga, Phys. Rev. D **105**, 063512 (2022).
[28] O. H. E. Philcox and M. M. Ivanov, Phys. Rev. D **105**, 043517 (2022).
[29] R. Scoccimarro, Astrophys. J. **544**, 597 (2000).
[30] E. Sefusatti, M. Crocce, S. Pueblas, and R. Scoccimarro, Phys. Rev. D **74**, 023522 (2006).
[31] T. Baldauf, L. Mercolli, M. Mirbabayi, and E. Pajer, J. Cosmol. Astropart. Phys. 05 (2015) 007.
[32] R. E. Angulo, S. Foreman, M. Schmittfull, and L. Senatore, J. Cosmol. Astropart. Phys. 10 (2015) 039.
[33] A. Eggemeier, R. Scoccimarro, and R. E. Smith, Phys. Rev. D **99**, 123514 (2019).
[34] M. M. Ivanov, M. Simonović, and M. Zaldarriaga, J. Cosmol. Astropart. Phys. 05 (2020) 042.
[35] G. D'Amico, J. Gleyzes, N. Kokron, D. Markovic, L. Senatore, P. Zhang, F. Beutler, and H. Gil-Marín, J. Cosmol. Astropart. Phys. 05 (2020) 005.
[36] A. Oddo, E. Sefusatti, C. Porciani, P. Monaco, and A. G. Sánchez, J. Cosmol. Astropart. Phys. 03 (2020) 056.
[37] A. Eggemeier, R. Scoccimarro, R. E. Smith, M. Crocce, A. Pezzotta, and A. G. Sánchez, Phys. Rev. D **103**, 123550 (2021).
[38] D. Alkhanishvili, C. Porciani, E. Sefusatti, M. Biagetti, A. Lazanu, A. Oddo, and V. Yankelevich, Mon. Not. R. Astron. Soc. **512**, 4961 (2022).
[39] A. Oddo, F. Rizzo, E. Sefusatti, C. Porciani, and P. Monaco, J. Cosmol. Astropart. Phys. 11 (2021) 038.
[40] S.-F. Chen, Z. Vlah, and M. White, J. Cosmol. Astropart. Phys. 02 (2022) 008.
[41] T. Baldauf, M. Garny, P. Taule, and T. Steele, Phys. Rev. D **104**, 123551 (2021).
[42] O. H. E. Philcox, Phys. Rev. D **103**, 103504 (2021).
[43] O. H. E. Philcox, Phys. Rev. D **104**, 123529 (2021).
[44] N. Aghanim et al. (Planck Collaboration), Astron. Astrophys. **641**, A6 (2020).
[45] D. Babich, P. Creminelli, and M. Zaldarriaga, J. Cosmol. Astropart. Phys. 08 (2004) 009.
[46] Note that we use the orthogonal template from Appendix B of Ref. [20], which has a physically correct suppression in the squeezed limit $k_1 \ll k_2 \approx k_3$, where it goes as $\mathcal{S}_{\mathrm{ortho}} \propto k_1/k_3$. It can be contrasted with the commonly used approximate template that features an unphysical enhancement in that limit [12].
[47] D. Baumann, A. Nicolis, L. Senatore, and M. Zaldarriaga, J. Cosmol. Astropart. Phys. 07 (2012) 051.

[48] J. J. M. Carrasco, M. P. Hertzberg, and L. Senatore, J. High Energy Phys. 09 (2012) 082.

[49] V. Desjacques, D. Jeong, and F. Schmidt, Phys. Rep. **733**, 1 (2018).

[50] T. Nishimichi, G. D'Amico, M. M. Ivanov, L. Senatore, M. Simonović, M. Takada, M. Zaldarriaga, and P. Zhang, Phys. Rev. D **102**, 123541 (2020).

[51] We suppress the explicit time dependence for brevity.

[52] E. Sefusatti and E. Komatsu, Phys. Rev. D **76**, 083004 (2007).

[53] E. Sefusatti, Phys. Rev. D **80**, 123002 (2009).

[54] A. Chudaykin, M. M. Ivanov, O. H. E. Philcox, and M. Simonović, Phys. Rev. D **102**, 063533 (2020).

[55] See Supplemental Material at http://link.aps.org/supplemental/10.1103/PhysRevLett.129.021301 for details on our theory model for the one-loop power spectrum and tree-level bispectrum, detailed plots that show both how the bispectrum allows to break the degeneracies between primordial non-Gaussianity and galaxy bias and the impact of primordial non-Gaussianity on the power spectrum, and a full triangle plot and constraint tables for our two analyses of the BOSS DR12 data.

[56] A. Taruya, K. Koyama, and T. Matsubara, Phys. Rev. D **78**, 123534 (2008).

[57] V. Assassi, D. Baumann, E. Pajer, Y. Welling, and D. van der Woude, J. Cosmol. Astropart. Phys. 11 (2015) 024.

[58] A. Moradinezhad Dizgah, M. Biagetti, E. Sefusatti, V. Desjacques, and J. Noreña, J. Cosmol. Astropart. Phys. 05 (2021) 015.

[59] V. Assassi, D. Baumann, and F. Schmidt, J. Cosmol. Astropart. Phys. 12 (2015) 043.

[60] R. Angulo, M. Fasiello, L. Senatore, and Z. Vlah, J. Cosmol. Astropart. Phys. 09 (2015) 029.

[61] Equilateral and orthogonal PNG produce identical scale-dependent biases that can be captured by a single free parameter.

[62] Defined by $P_{11}(k_{NL})k_{NL}^3/(2\pi^2) = 1$.

[63] E. Pajer and M. Zaldarriaga, J. Cosmol. Astropart. Phys. 08 (2013) 037.

[64] For local-type PNG the situation is different: the PNG bias terms dominate on large scales.

[65] M. M. Ivanov, M. Simonović, and M. Zaldarriaga, Phys. Rev. D **101**, 083504 (2020).

[66] L. Senatore and M. Zaldarriaga, J. Cosmol. Astropart. Phys. 02 (2015) 013.

[67] T. Baldauf, M. Mirbabayi, M. Simonović, and M. Zaldarriaga, Phys. Rev. D **92**, 043514 (2015).

[68] D. Blas, M. Garny, M. M. Ivanov, and S. Sibiryakov, J. Cosmol. Astropart. Phys. 07 (2016) 052.

[69] D. Blas, M. Garny, M. M. Ivanov, and S. Sibiryakov, J. Cosmol. Astropart. Phys. 07 (2016) 028.

[70] M. M. Ivanov and S. Sibiryakov, J. Cosmol. Astropart. Phys. 07 (2018) 053.

[71] A. Vasudevan, M. M. Ivanov, S. Sibiryakov, and J. Lesgourgues, J. Cosmol. Astropart. Phys. 09 (2019) 037.

[72] C. Alcock and B. Paczynski, Nature (London) **281**, 358 (1979).

[73] S. Alam et al. (BOSS Collaboration), Mon. Not. R. Astron. Soc. **470**, 2617 (2017).

[74] M. M. Ivanov, O. H. E. Philcox, M. Simonović, M. Zaldarriaga, T. Nishimichi, and M. Takada, Phys. Rev. D **105**, 043531 (2022).

[75] O. H. E. Philcox, M. M. Ivanov, M. Simonović, and M. Zaldarriaga, J. Cosmol. Astropart. Phys. 05 (2020) 032.

[76] F.-S. Kitaura et al., Mon. Not. R. Astron. Soc. **456**, 4156 (2016).

[77] M. Simonović, T. Baldauf, M. Zaldarriaga, J. J. Carrasco, and J. A. Kollmeier, J. Cosmol. Astropart. Phys. 04 (2018) 030.

[78] R. J. Cooke, M. Pettini, and C. C. Steidel, Astrophys. J. **855**, 102 (2018).

[79] F. Schmidt and M. Kamionkowski, Phys. Rev. D **82**, 103002 (2010).

[80] K. Akitsu, G. Cabass, M. M. Ivanov, O. H. E. Philcox, M. Simonović, and M. Zaldarriaga (to be published).

[81] A. Barreira, T. Lazeyras, and F. Schmidt, J. Cosmol. Astropart. Phys. 08 (2021) 029.

[82] T. Lazeyras, A. Barreira, and F. Schmidt, J. Cosmol. Astropart. Phys. 10 (2021) 063.

[83] Notice that flat priors on (f_{NL}^{equil}, f_{NL}^{ortho}) do not respect the physical conditions $0 \le c_s^2 \le 1$; see Eq. (5) and Ref. [20].

[84] R. Laureijs et al. (Euclid Collaboration), arXiv:1110.3193.

[85] A. Aghamousa et al. (DESI Collaboration), arXiv:1611.00036.

[86] R. Scoccimarro, Phys. Rev. D **92**, 083532 (2015).

[87] O. H. E. Philcox, J. Hou, and Z. Slepian, arXiv:2108.01670.

[88] D. J. Schlegel et al., arXiv:1907.11171.

[89] https://github.com/Michalychforever/CLASS-PT and https://github.com/oliverphilcox/full_shape_likelihoods.

[90] D. Blas, J. Lesgourgues, and T. Tram, J. Cosmol. Astropart. Phys. 07 (2011) 034.

[91] B. Audren, J. Lesgourgues, K. Benabed, and S. Prunet, J. Cosmol. Astropart. Phys. 02 (2013) 001.

[92] T. Brinckmann and J. Lesgourgues, Phys. Dark Universe **24**, 100260 (2019).

[93] https://getdist.readthedocs.io/en/latest/.

[94] A. Lewis, arXiv:1910.13970.